White Rose Research Online

eprints@whiterose.ac.uk
https://eprints.whiterose.ac.uk
Universities of Leeds, Sheffield and York

Deposited via The University of Leeds.

White Rose Research Online URL for this paper:
https://eprints.whiterose.ac.uk/id/eprint/74786/

Article:
Rucklidge, AM and Rucklidge, WJ (2003) Convergence properties of the 8, 10 and 12 mode representations of quasipatterns. Physica D: Nonlinear Phenomena, 178 (1-2). pp. 62-82. ISSN: 0167-2789

https://doi.org/10.1016/S0167-2789(02)00792-3

© 2003, Elsevier. Licensed under the Creative Commons Attribution-NonCommercial-NoDerivatives 4.0 International http://creativecommons.org/licenses/by-nc-nd/4.0/

Reuse
Items deposited in White Rose Research Online are protected by copyright, with all rights reserved unless indicated otherwise. They may be downloaded and/or printed for private study, or other acts as permitted by national copyright laws. The publisher or other rights holders may allow further reproduction and re-use of the full text version. This is indicated by the licence information on the White Rose Research Online record for the item.

Takedown
If you consider content in White Rose Research Online to be in breach of UK law, please notify us by emailing eprints@whiterose.ac.uk including the URL of the record and the reason for the withdrawal request.

White Rose Consortium ePrints Repository
http://eprints.whiterose.ac.uk/

This is an author produced version of a paper published in **Physica D: Nonlinear Phenomena**. This paper has been peer-reviewed but does not include final publisher proof-corrections or journal pagination.

White Rose Repository URL for this paper:
http://eprints.whiterose.ac.uk/archive/00000997/

Citation for the published paper
Rucklidge, A.M. and Rucklidge, W.J. (2003) *Convergence properties of the 8, 10 and 12 mode representations of quasipatterns.* Physica D: Nonlinear Phenomena, 178 (1-2). pp. 62-82.

Citation for this paper
To refer to the repository paper, the following format may be used:

Rucklidge, A.M. and Rucklidge, W.J. (2003) *Convergence properties of the 8, 10 and 12 mode representations of quasipatterns.* Author manuscript available at: http://eprints.whiterose.ac.uk/archive/00000997/ [Accessed: *date*].
Published in final edited form as:

Rucklidge, A.M. and Rucklidge, W.J. (2003) *Convergence properties of the 8, 10 and 12 mode representations of quasipatterns.* Physica D: Nonlinear Phenomena, 178 (1-2). pp. 62-82.

White Rose Consortium ePrints Repository
eprints@whiterose.ac.uk

Physica D **178** (2003) 62–82

Convergence properties of the 8, 10 and 12 mode representations of quasipatterns

A.M. Rucklidge

Department of Applied Mathematics, University of Leeds, Leeds LS2 9JT, UK

and

W.J. Rucklidge

148 Promethean Way, Mountain View, CA 94043, USA

Abstract

Spatial Fourier transforms of quasipatterns observed in Faraday wave experiments suggest that the patterns are well represented by the sum of 8, 10 or 12 Fourier modes with wavevectors equally spaced around a circle. This representation has been used many times as the starting point for standard perturbative methods of computing the weakly nonlinear dependence of the pattern amplitude on parameters. We show that nonlinear interactions of n such Fourier modes generate new modes with wavevectors that approach the original circle no faster than a constant times n^{-2}, and that there are combinations of modes that do achieve this limit. As in KAM theory, small divisors cause difficulties in the perturbation theory, and the convergence of the standard method is questionable in spite of the bound on the small divisors. We compute steady quasipattern solutions of the cubic Swift–Hohenberg equation up to 33^{rd} order to illustrate the issues in some detail, and argue that the standard method does not converge sufficiently rapidly to be regarded as a reliable way of calculating properties of quasipatterns.

Key words: Pattern formation, quasipatterns, Faraday waves, small divisors.
47.20.Ky, 47.54.+r, 61.44.Br.

1 Introduction

Experimental observations of regular patterns have been widely reported in many physical systems, for example, Rayleigh–Bénard convection, reaction–diffusion problems and the Faraday wave experiment [1,2]. In the last example, a tray containing a layer of fluid is subjected to vertical vibrations, and the flat horizontal surface of the fluid becomes unstable once the amplitude of the vibration exceeds a critical value. With multi-frequency forcing, this experiment is capable of producing a wide variety of patterns with an astonishing degree of symmetry [3].

The simplest patterns: stripes, squares and hexagons, have reflection, rotation and translation symmetries, and a comprehensive theory has been developed to analyse the creation of these patterns from the initial flat state [4]. In order to apply the theory to the experiments, two idealisations are necessary. First, the experimental boundaries are ignored, and so in effect the experiment is supposed to be taking place in a container of infinite size: there are two unbounded spatial directions; and second, the observed pattern is supposed to have perfect spatial periodicity. Restricting to a spatially periodic subdomain enables rigorous theory to be applied [5], and the existence of stripe, square, and hexagon (and other) solutions of model partial differential equations (PDEs) can be proven using equivariant bifurcation theory [4]. Given that in some highly controlled experiments the idealisation of spatial periodicity appears to hold over dozens of wavelengths of the pattern, these assumptions are perfectly reasonable when the objective is to understand the nature of these periodic patterns.

However, experiments are quite capable of producing patterns that cannot be analysed in this way. Notable examples of this include *quasipatterns*, which are quasiperiodic in any spatial direction, that is, the amplitude of the pattern (taken along any direction in the plane) can be regarded as a sum of waves with incommensurate spatial frequencies. Experimental photographs of quasipatterns are reproduced in figure 1(a–c) from [3]; the lack of spatial periodicity can be seen in the images, and the long range rotational order is evident from the spatial Fourier transforms, in a manner similar to quasicrystals [6]. The Faraday wave experiment has been a particularly fruitful source of quasipatterns since they were discovered by Christiansen et al. [7] (8-fold

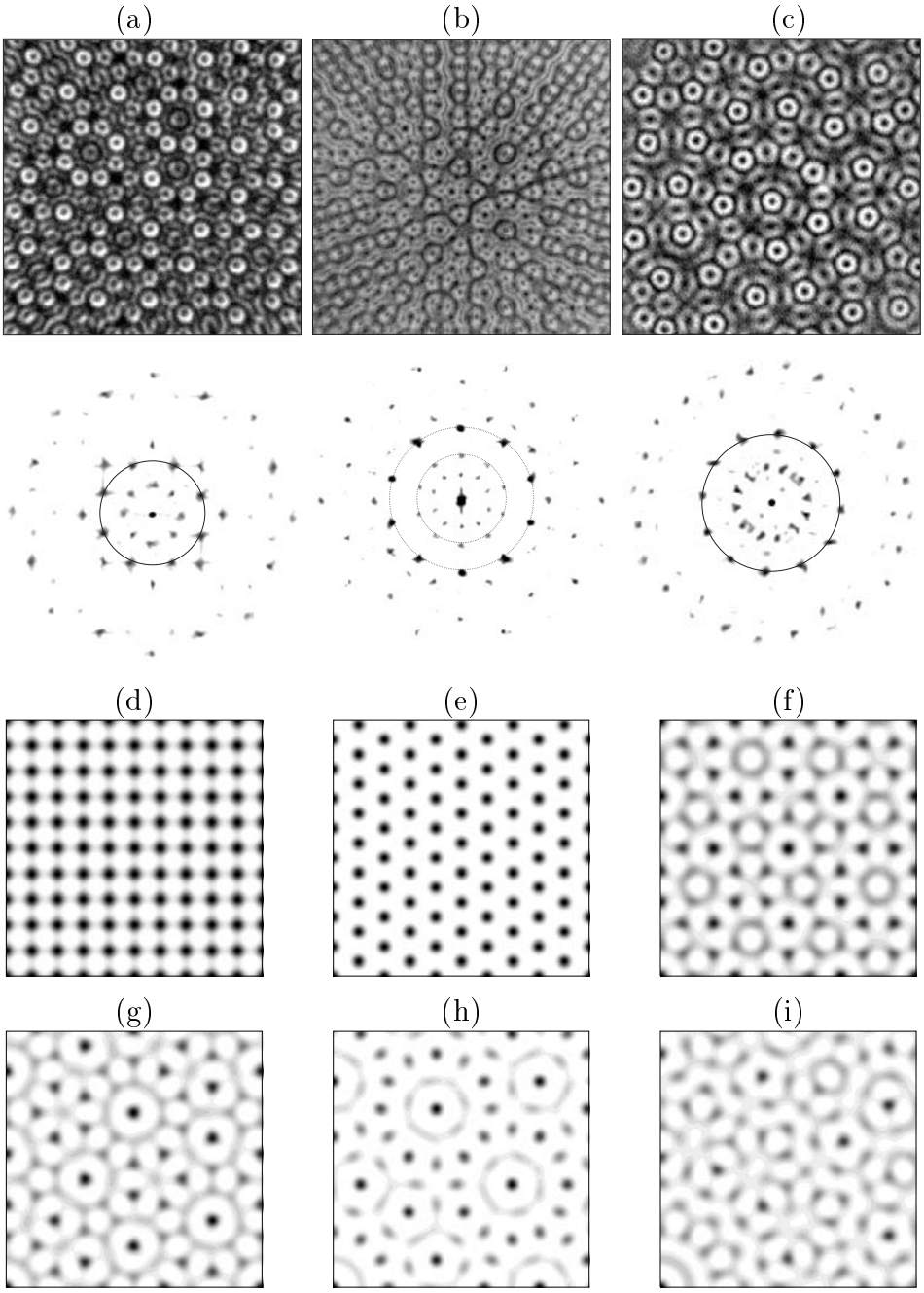

Fig. 1. (a–c) Experimental observation of (a) 8-fold, (b) 10-fold, and (c) 12-fold quasipatterns in the Faraday wave experiment with (a) 3 and (b,c) 2 frequency forcing. Top line: experimental photographs; bottom line: spatial Fourier transform. The circles in the Fourier spectra indicate wavenumbers that are excited by one of the harmonics in the forcing (both harmonics in case b). From Arbell and Fineberg (2002) [3], with permission. (d–i) Synthetic examples of periodic patterns (d,e) with $Q = 4$, 6 wavevectors with equal amplitudes, and quasipatterns (f,g,h,i) with $Q = 8$, 10, 12, 14 wavevectors.

quasipattern with single frequency forcing and a relatively low viscosity fluid) and Edwards and Fauve [8,9] (12-fold quasipattern with two frequency forcing and a high viscosity fluid). See references [3,10–12] for further large aspect ratio experiments, and [13] for a recent review of experimental and theoretical issues. Quasipatterns have also been reported in studies of nonlinear optical systems [14,15], and in numerical studies of several model PDEs [16–18], though of course computations carried out in large periodic domains can only approximate a quasiperiodic pattern.

The forcing in Faraday wave experiments can be a simple sinusoid, but quasipatterns are more readily generated when two or three commensurate temporal frequencies are included in the forcing. Each frequency excites, or nearly excites, waves with a particular wavenumber, and nonlinear resonant interactions between these waves, as well as waves that damped, can be used to encourage or discourage particular waves to appear in the pattern [9,19–21]. By tuning such parameters as the driving frequency, the fluid viscosity and the layer depth, experimentalists have been able to produce very clean examples of quasipatterns (as in figure 1a–c), as well as to demonstrate a clear understanding of the physical mechanisms behind their production.

Since quasipatterns, by their very nature, do not fit into periodic domains, equivariant bifurcation theory cannot be applied, and other methods are required in order to predict, for example, the dependence of the amplitude of the quasipattern on parameters, or the stability of the quasipattern. One approach, which has been followed many times, is to suppose that the dynamics of the quasipattern is dominated by the evolution of the amplitudes of Q waves (Q even), with wavevectors distributed equally around a circle. Equations governing the evolution of these amplitudes can readily be written down, and take the form

$$\dot{A}_j = \mu A_j + \sum_{k=1}^{Q/2} \beta_{j,k} \left|A_k\right|^2 A_j + \text{resonant terms}, \tag{1}$$

where A_j is the complex amplitude of mode j, μ describes the forcing of the pattern, and the $\beta_{j,k}$ coefficients depend on the angle between the wavevectors of modes j and k. Resonant terms (depending on the value of Q) are also included but not written explicitly above. Steady solutions of (1) with all amplitudes equal represent patterns of the type shown in figure 1(d–i), for

$Q = 4, \ldots, 14$ wavevectors.

Equation (1) can be written down directly from symmetry or general physical considerations [22–25], but it has also been derived from PDEs that model the hydrodynamic and other problems [26–29]. The method that is used is called modified perturbation theory [30,31], and the amplitude equation (1) is only the leading order approximation to the equations that govern the evolution of the amplitudes of the modes.

The problem with this approach when applied to quasipatterns is that it overlooks the near-singular resonances that small divisors can cause, and ignores the nearly neutral modes that are driven by high-order nonlinear interactions.

The difficulty of small divisors arises in a variety of situations as well as this one, for example, the persistence of quasiperiodic oscillations in Hamiltonian systems, the analysis of which cumulated in the KAM theorem (cf. [32]). To take an illustrative example, consider the one-dimensional ordinary differential equation with quasiperiodic forcing:

$$\frac{da}{dt} = \sum_{m_1,m_2=-\infty}^{\infty} C_{m_1,m_2} e^{i(m_1\omega_1 + m_2\omega_2)t}, \tag{2}$$

where C_{m_1,m_2} are constants satisfying $C_{0,0} = 0$ and $C_{m_1,m_2} \leq K_1 \left(|m_1| + |m_2|\right)^{-\gamma}$ for every pair of integers m_1 and m_2, with $\gamma > 2$ so that the sum converges. The frequencies ω_1 and ω_2 are incommensurate. This series can be integrated formally term by term to give:

$$a(t) = \sum_{m_1,m_2=-\infty}^{\infty} \frac{C_{m_1,m_2}}{i(m_1\omega_1 + m_2\omega_2)} e^{i(m_1\omega_1 + m_2\omega_2)t}. \tag{3}$$

It is clear that this sum for $a(t)$ may not converge even if the sum for the forcing function does, since $m_1\omega_1 + m_2\omega_2$ comes arbitrarily close to zero, and so the amplitudes of the Fourier coefficients can be arbitrarily large. However, if ω_1 and ω_2 satisfy a Diophantine condition, that is, if there are constants $K_2 > 0$ and $\delta > 0$ such that ω_1 and ω_2 satisfy

$$|m_1\omega_1 + m_2\omega_2| \geq K_2 \left(|m_1| + |m_2|\right)^{-\delta} \tag{4}$$

for every m_1 and m_2, then the sum for $a(t)$ can readily be shown to converge

provided $\gamma > 2 + \delta$. This increases the constraints on the smoothness of the forcing function. Normally, integrating a Fourier series poses no difficulties, but this example demonstrates that when quasiperiodic functions are involved, an extra degree of caution is necessary.

Currently, there is no KAM-like theory for quasipatterns, which are quasiperiodic in two dimensions (x, y), rather than than the usual one dimension (time). There is, however, a theory for one-dimensional steady quasipatterns [33], which makes use of space as a time-like evolution variable. In the absence of a rigorous theory for two-dimensional quasipatterns, we examine the issue of convergence or otherwise of the standard method of computing amplitude equations of the form of (1), when applied to quasipatterns.

In section 2, we revisit the standard method of modified perturbation theory as applied to the computation of the amplitude of a quasipattern as a function of a parameter close to the onset of the pattern, and point out where the problem of small divisors arises. In section 3, we work out just how small the small divisors are (with numerical results that make use of a rapid method presented in Appendix A), and in section 4 return to general issue of convergence. We discuss the specific example of the Swift–Hohenberg equation in section 5, and conclude in section 6 with the argument that the standard method does not appear to converge sufficiently rapidly to be regarded as a reliable way of calculating properties of quasipatterns.

2 Perturbation theory

In order to point out exactly where the difficulties lie, we begin by going through the standard modified perturbation theory [30,31] for a general pattern-forming PDE:

$$\frac{\partial U}{\partial t} = \mathcal{F}_\mu(U) = \mathcal{L}_\mu(U) + \mathcal{N}_\mu(U), \tag{5}$$

where $U(x, y, t)$ represents the order parameter (or any measure of the pattern), $\mathcal{F}_\mu$ is an operator containing spatial derivatives that depends on a parameter μ and that can be split into linear ($\mathcal{L}_\mu$) and nonlinear ($\mathcal{N}_\mu$) parts. The order parameter may be multi-dimensional. A specific example is the

Swift–Hohenberg equation [34]:

$$\frac{\partial U}{\partial t} = \mu U - (1 + \nabla^2)^2 U - U^3, \tag{6}$$

where $U(x, y, t) \in \mathbb{R}$, but many pattern-forming problems can be cast into this form, or variations [35].

The spatially uniform trivial state $U(x, y, t) = 0$ is always a possible solution, but it loses stability as the parameter μ increases through a critical value μ_0, which we take to be zero. We focus on the case where the mode that becomes unstable is a Fourier mode with nonzero wavenumber, which we scale to 1. The problem is posed on the whole plane, so $(x, y) \in \mathbb{R}^2$, but if we were interested only in spatially periodic solutions, then the whole plane could be restricted to a periodic domain, and standard equivariant bifurcation theory [4] could be used. However, this rules out the spatially quasiperiodic patterns of interest here.

Instead of equivariant bifurcation theory, we use the older technique of modified perturbation theory [30,31], and suppose that the parameter μ is close to its critical value $\mu_0 = 0$, that the amplitude of the solution is small and that the pattern evolves slowly. We introduce a small parameter ϵ, scale time by ϵ^{-1}, and write

$$U = \epsilon U_1 + \epsilon^2 U_2 + \epsilon^3 U_3 + \ldots, \qquad \mu = \epsilon \mu_1. \tag{7}$$

Then $\mathcal{L}_\mu(U)$ is of order ϵ, and $\partial U/\partial T$ and $\mathcal{N}_\mu(U)$ are of order ϵ^2. In many examples, there are additional symmetries in the problem, and it may be necessary to scale time by ϵ^{-2} and set $\mu = \epsilon^2 \mu_2$ if it turns out that $\mu_1 = 0$. We focus on the general case here, treating the specific example of the Swift–Hohenberg equation in section 5.

The leading order equation, at order ϵ, is

$$\mathcal{L}_0(U_1) = 0. \tag{8}$$

In the Swift–Hohenberg example, the operator $\mathcal{L}_0$ would be $-(1 + \nabla^2)^2$. Since $\mu = 0$ is a bifurcation point, the linear operator $\mathcal{L}_0$ is singular with a circle of marginally stable Fourier modes in its kernel: $\mathcal{L}_0(e^{i\boldsymbol{k}\cdot\boldsymbol{x}}) = 0$ whenever $k =$

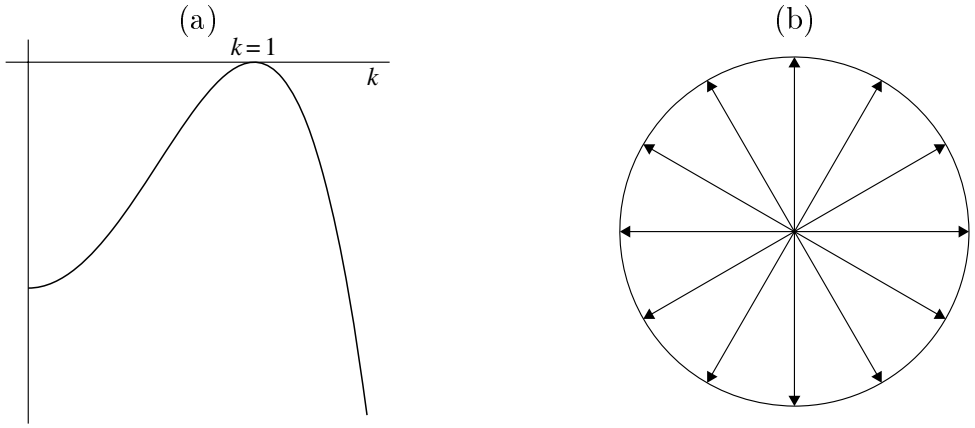

Fig. 2. (a) Schematic growth (decay) rate of a mode $e^{i\boldsymbol{k}\cdot\boldsymbol{x}}$, as a function of $k = |\boldsymbol{k}|$ at $\mu = 0$. Modes with $k = 1$ are marginally stable. (b) $Q = 12$ wavevectors on the circle $k = 1$.

$|\boldsymbol{k}| = 1$, (see figure 2a) and so (8) has nontrivial solutions of the form

$$U_1(x, y, t) = \sum_{j=1}^{Q} A_j(t) e^{i\boldsymbol{k}_j\cdot\boldsymbol{x}}, \tag{9}$$

where we can select any Q wavevectors $\boldsymbol{k}_j$, with $j = 1, \ldots, Q$, from the circle $k = 1$ (figure 2b).

In principle, any set of unit length wavevectors is permitted, though if U is required to be real, the negative of each vector must also be included. The usual choice for periodic patterns is $Q = 2$, 4 or 6 equally spaced wavevectors, for stripes, squares or hexagons, though $Q = 8$, 10 and 12 have also been used in previous studies and have been observed in experiments. Synthetic examples of patterns and quasipatterns with $A_j =$ constant for $Q = 4, \ldots, 14$ are shown in figure 1(d–i).

At each higher order in ϵ, the equation to solve takes the form

$$\mathcal{L}_0(U_n) = -\mathcal{N}_n(U_1, \ldots, U_{n-1}; \mu_1) + \frac{\partial U_{n-1}}{\partial t}, \tag{10}$$

where the term $\mathcal{N}_n$ is given by the order ϵ^n part of Taylor expansion of $\mathcal{F}_\mu(U)$ in powers of ϵ, so it contains nonlinear terms and the parameter μ_1 from $\mathcal{L}_\mu(U)$. In principle, the equations can be solved order by order, with each U_n determined by $U_1, \ldots, U_{n-1}$. At each order, the nonlinear terms $\mathcal{N}_2$, $\mathcal{N}_3$, etc., involve quadratic, cubic, etc., combinations of the original Fourier modes, which

implies that these terms will involve powers of (at most) n in the original amplitudes, and that the Fourier spectrum of $\mathcal{N}_n$ contains wavevectors made up (at most) of all combinations of up to n of the original wavevectors in the set K. If we let

$$\boldsymbol{k}_{\boldsymbol{m}} = \sum_{j=1}^{Q} m_j \boldsymbol{k}_j, \qquad \text{where} \qquad \boldsymbol{m} \in \mathbb{Z}^Q, \tag{11}$$

then the wavevectors in the nonlinear terms at order n are all those with $\boldsymbol{k}_{\boldsymbol{m}}$ satisfying $|\boldsymbol{m}| = \sum_j |m_j| \leq n$.

In order to solve the equation (10) at order n, the modes present in $\mathcal{N}_n$ are divided into two classes. First, if a mode has wavevector on the unit circle, then, using the orthogonality in $\mathbb{R}^2$ of Fourier modes with different wavevectors (or, more properly, using solutions of the adjoint equation and integrating over $\mathbb{R}^2$), the coefficient of this mode on the RHS of (10) must be zero (this condition is known as a solvability condition). The reason for this is that $\mathcal{L}_0(e^{i\boldsymbol{k}\cdot\boldsymbol{x}})$ is zero if $|\boldsymbol{k}| = 1$, and so such modes are not present in the LHS of (10). So, for example, the evolution of the amplitudes $A_j(t)$ is determined at second order and takes the general form:

$$\dot{A}_j = f_j(A_1, \ldots, A_Q; \mu_1), \tag{12}$$

where the dot stands for evolution on the slow time scale. These evolution equations will contain only terms linear and quadratic in the A's. In examples with additional symmetry (or with $Q \neq 6$ and $Q \neq 12$ equally spaced modes), this equation is vacuous, with $\mu_1 = 0$ and $U_2 = 0$, and the evolution of the amplitudes $A_j(t)$ is determined at third order – see section 5.

Once the modes on the unit circle have been removed by satisfying a solvability condition, all remaining modes in $\mathcal{N}_n$ (making up the second class of modes) have wavevectors off the unit circle. For these modes, $\mathcal{L}_0(e^{i\boldsymbol{k}\cdot\boldsymbol{x}})$ is nonzero, so the singular linear operator operator $\mathcal{L}_0$ can be inverted to give U_n:

$$U_n = \mathcal{L}_0^{-1}\left(-\mathcal{N}_n(U_1, \ldots, U_{n-1}; \mu_1) + \frac{\partial U_{n-1}}{\partial t}, \right). \tag{13}$$

Inverting the operator $\mathcal{L}_0$ generates arbitrary linear combinations of modes in its kernel that are used to satisfy solvability conditions at higher order. Like

the nonlinear term $\mathcal{N}_n$, each U_n will include modes with wavevectors made up of (at most) of all combinations $\boldsymbol{k_m}$ of up to n of the original wavevectors, with $|\boldsymbol{m}| \leq n$.

As well as the method outlined above, there are two other approaches to these computations, both of which avoid adding modes on the unit circle at each order when inverting $\mathcal{L}_0$. First, the original paper [30] used an expansion for the parameter μ: $\mu = \epsilon\mu_1 + \epsilon^2\mu_2 + \ldots$, and chose values of μ_1, μ_2, etc., to satisfy the solvability conditions at each order. As a result, for a given value of μ, a polynomial for ϵ must be solved before the amplitude can be computed. In the second alternative, the original $\mu = \epsilon\mu_1$ is used, leaving modes in the RHS of (10) on the unit circle, which cannot be removed. The modes involved will be exactly the Q modes that were taken in the original ansatz for U_1, and the contributions that appear in (10) can be redesignated as order ϵ^{n-1} corrections to the leading order solvability condition (12). We have checked for some specific examples that the three approaches give the same results, but prefer the approach described in detail for the problem at hand.

In many cases, the leading order solvability condition (12) is sufficient, but in other problems, this equation is degenerate, and the calculation is carried to some higher order N in powers of ϵ. An implicit *assumption* is that the power series expansion (7) for U converges for some nonzero ϵ as this process is repeated (and $N \to \infty$). At each order n in the perturbation calculation, the operator $\mathcal{L}_0$ must be inverted for each mode $e^{i\boldsymbol{k_m}\cdot\boldsymbol{x}}$, where $|\boldsymbol{m}| \leq n$ and $\boldsymbol{k_m}$ could be close to the unit circle. In typical pattern forming problems, the growth rate of a mode $e^{i\boldsymbol{k}\cdot\boldsymbol{x}}$ has a quadratic maximum at $k = 1$ (see figure 2a), so

$$\mathcal{L}_0^{-1}\left(e^{i\boldsymbol{k}\cdot\boldsymbol{x}}\right) \approx -\frac{1}{(1-|\boldsymbol{k}|^2)^2}e^{i\boldsymbol{k}\cdot\boldsymbol{x}}, \tag{14}$$

for $|\boldsymbol{k}|$ close to 1, with equality in the case of the Swift–Hohenberg example. For periodic patterns (with $Q = 2$, 4 or 6 modes), integer combinations of the initial wavevectors form a lattice, so the wavevectors $\boldsymbol{k_m}$ cannot come arbitrarily close to the unit circle (apart from the modes on the unit circle, which are dealt with by applying solvability conditions). In this case, convergence will not be a problem for small enough ϵ. However, for quasipatterns (with $Q = 8$, 10, 12 or more modes), there is no lattice and combinations of modes can come arbitrarily close to the unit circle, leading to *small divisors*

in the denominator when $\mathcal{L}_0$ is inverted. The issue of convergence has never been properly examined for two-dimensional quasipatterns, and most authors assume that the leading order solvability condition (12) yields useful and reliable information about the amplitude and stability of the quasipattern. We will see below that it is far from obvious that this is the case.

This so-called small divisor problem is well known in other situations that feature quasiperiodicity, and, in particular, is known to arise with these quasipatterns. What is not known is how rapidly $\mathcal{L}_0^{-1}$ grows as the order of truncation N increases. The question here is how close $\boldsymbol{k_m}$ can get to the unit circle as $|\boldsymbol{m}| = N$ becomes large, and does the power series expansion for U have a nonzero radius of convergence in spite of the bad behaviour of $\mathcal{L}_0^{-1}$. We turn to these two questions in the next sections.

3 Combinations of modes

In this section, we take integer combinations of up to N of the Q original vectors on the unit circle, and compute how close these combinations can get to the unit circle as N becomes large. We are able to prove that the closest $|\boldsymbol{k_m}|$ can get to 1, with $|\boldsymbol{m}| = N$, is bounded above and below by a constant times N^{-2} in the cases $Q = 8$, 10 and 12. We also have numerical evidence that the closest distance is bounded above and below by a constant times N^{-4} in the case $Q = 14$ (at least for $N \leq 1000$), going to zero much more rapidly than in the other three cases.

We begin with figure 3(a–f), illustrating the locations of combinations of up to $N = 7$, 11 and 15 wavevectors in the case $Q = 12$. Note how the density of points increases with N, and how the minimum distance between points and the unit circle goes down with N. Figure 3(g–i) compares with the cases $Q = 8$ and 10, which show similar behaviour, and with $Q = 14$, which has a much higher density of possible wavevectors for the same value of N.

Figure 4 shows detailed numerical results for the smallest nonzero distance $||\boldsymbol{k_m}| - 1|$ from the unit circle as a function of the total number of modes $|\boldsymbol{m}| = N$ for $Q = 8$, 10, 12 and 14 original modes. The calculations are made possible by a rapid method of searching for the closest approach, presented in appendix A: the method is order N^2 for $Q = 8$, 10, 12 and order N^4 for

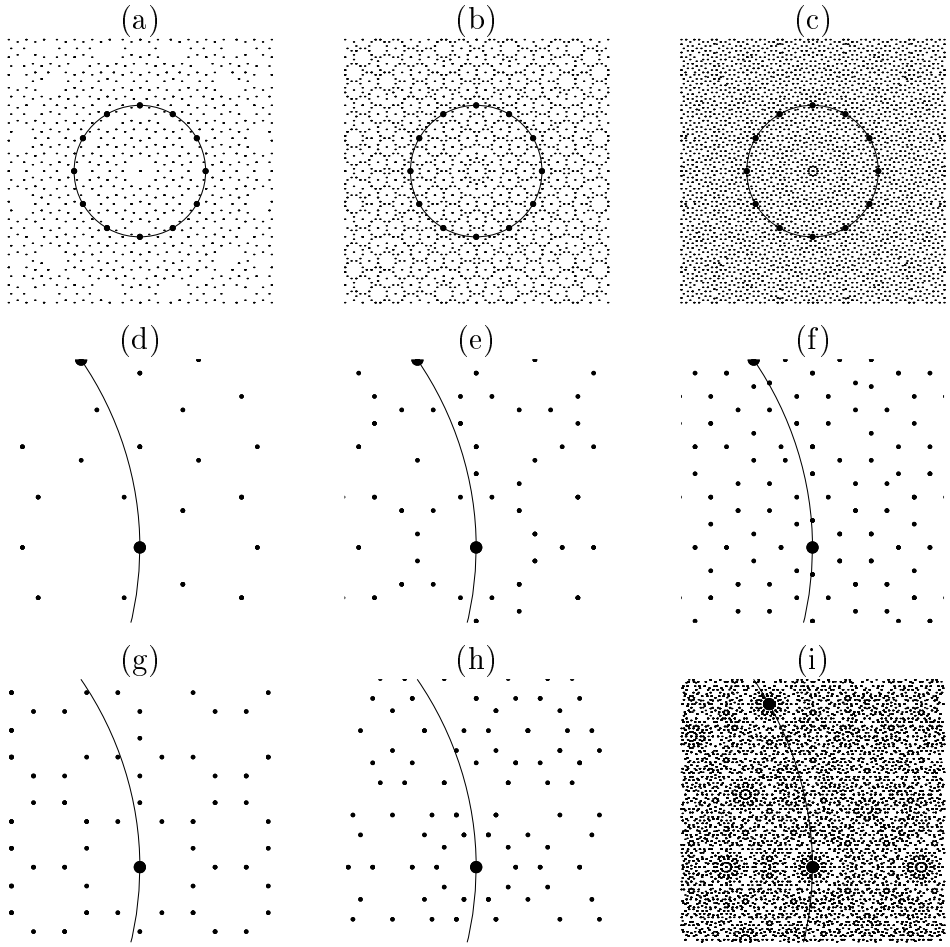

Fig. 3. Positions of combinations of up to N wavevectors original vectors on the unit circle, with (a) $Q = 12$, $N = 7$, (b) $Q = 12$, $N = 11$, (c) $Q = 12$, $N = 15$; (d,e,f) on second row: details of first row. The circle indicates the unit circle, $k = 1$, the large dots are the original Q wavevectors, and the small dots are integer combinations of these. (g), (h) and (i) show $N = 15$ and $Q = 8$, 10 and 14. Note how the density of points increases with N and with Q, and the proximity of points to the unit circle decreases with N. Note also how the density of points is markedly higher with $Q = 14$, for the same value of N.

$Q = 14$. The solid lines in figure 4 confirm numerically that the scaling for the distance to the unit circle is order N^{-2} for $Q = 8$, 10 and 12, and order N^{-4} for $Q = 14$. The remainder of this section is devoted to proving the correctness of the N^{-2} scalings, and in particular, to showing how for certain values of N, wavevectors close to the unit circle can be found explicitly in the cases $Q = 8$, 10 and 12, using continued fraction expansions.

We label the vectors $\boldsymbol{k}_1$, $\boldsymbol{k}_2$, ..., $\boldsymbol{k}_Q$ anticlockwise around the circle starting with $\boldsymbol{k}_1 = (1, 0)$, with $\boldsymbol{k}_{j+Q/2} = -\boldsymbol{k}_j$. We are interested in the scal-

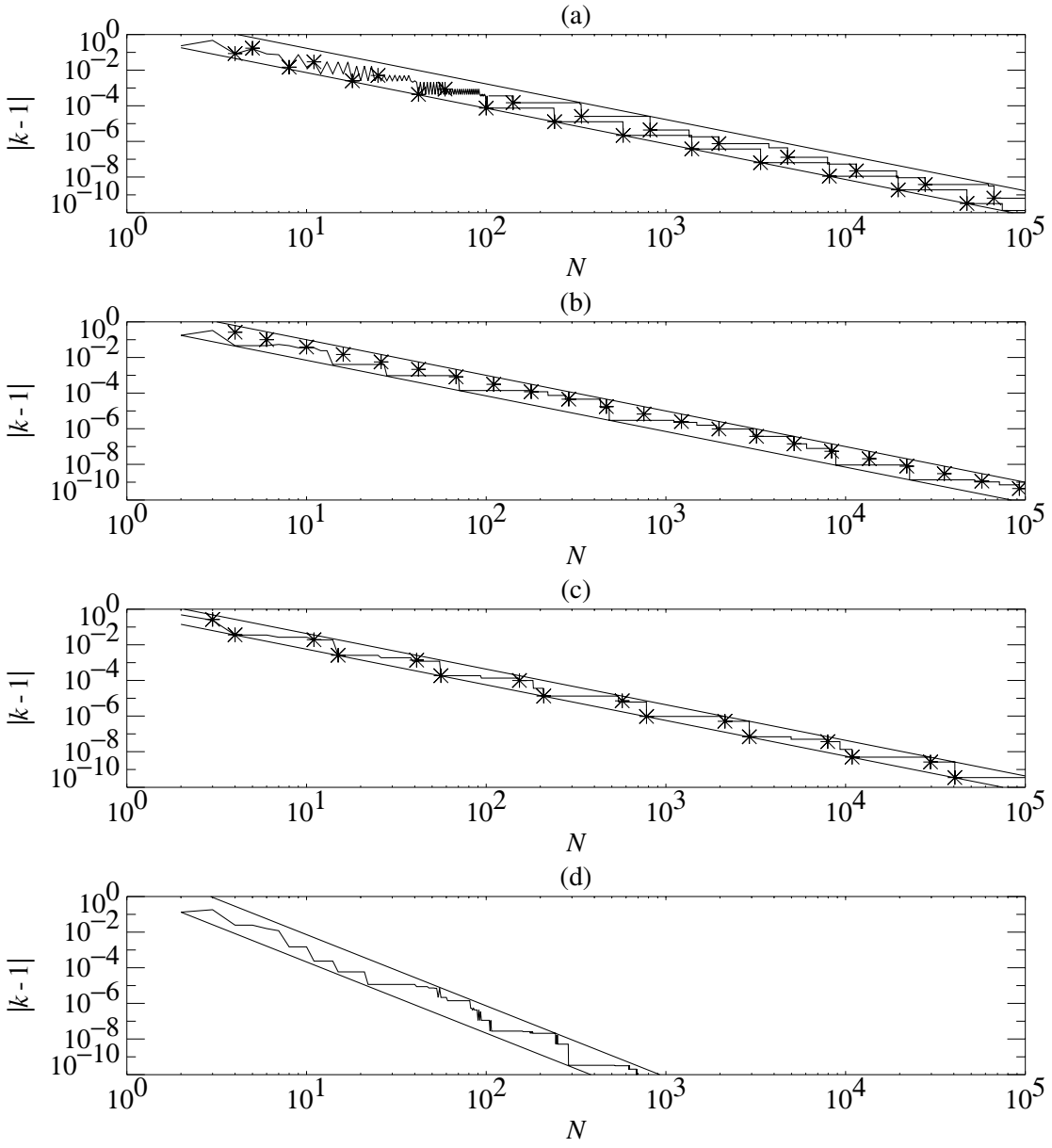

Fig. 4. Smallest nonzero distances from the unit circle $||\boldsymbol{k_m}| - 1|$ as a function of the total number of modes $|\boldsymbol{m}| = N$, for (a) $Q = 8$, (b) $Q = 10$, (c) $Q = 12$ and (d) $Q = 14$. Stars in (a–c) mark distances calculated from equations (24–26), and straight lines indicate the scaling N^{-2}. The two staircase-shaped lines in (a) indicate minimum distances for even and odd values of N. The straight lines in (d) indicate N^{-4}.

ing behaviour of how close $\boldsymbol{k_m} = \sum_{j=1}^{Q} m_j \boldsymbol{k}_j$ can get to the unit circle as $|\boldsymbol{m}| = \sum_j |m_j| = N$ becomes large, so we seek the vector of integers $\boldsymbol{m}$ with $|\boldsymbol{m}| = N$ that yields the vector $\boldsymbol{k_m}$ that is closest to the unit circle for this value of N. Once we have found a particular vector that is close to the unit

circle, we are also interested in finding the smallest N that can achieve this distance. Including equal and opposite vectors $\boldsymbol{k}_j$ and $\boldsymbol{k}_{j+Q/2}$ will only increase N without coming any closer to the unit circle, so we take only $m_1, \ldots, m_{Q/2}$ but allow these to be negative.

With this restriction, the squared length of a vector $\boldsymbol{k_m}$ is, for each value of Q:

$$
\begin{aligned}
Q = 2: \quad & |\boldsymbol{k_m}|^2 = m_1^2 \\
Q = 4: \quad & |\boldsymbol{k_m}|^2 = m_1^2 + m_2^2 \\
Q = 6: \quad & |\boldsymbol{k_m}|^2 = m_1^2 + m_2^2 + m_3^2 + m_1 m_2 + m_2 m_3 - m_3 m_1 \\
Q = 8: \quad & |\boldsymbol{k_m}|^2 = m_1^2 + m_2^2 + m_3^2 + m_4^2 \\
& \qquad + \sqrt{2}(m_1 m_2 + m_2 m_3 + m_3 m_4 - m_4 m_1) \\
Q = 10: \quad & |\boldsymbol{k_m}|^2 = m_1^2 + m_2^2 + m_3^2 + m_4^2 + m_5^2 \\
& \qquad + \omega(m_1 m_2 + m_2 m_3 + m_3 m_4 + m_4 m_5 - m_5 m_1) \\
& \qquad + (\omega - 1)(m_1 m_3 + m_2 m_4 + m_3 m_5 - m_4 m_1 - m_5 m_2) \\
Q = 12: \quad & |\boldsymbol{k_m}|^2 = m_1^2 + m_2^2 + m_3^2 + m_4^2 + m_5^2 + m_6^2 \\
& \qquad + m_1 m_3 + m_2 m_4 + m_3 m_5 + m_4 m_6 - m_5 m_1 - m_6 m_2 \\
& \qquad + \sqrt{3}(m_1 m_2 + m_2 m_3 + m_3 m_4 + m_4 m_5 + m_5 m_6 - m_6 m_1) \\
Q = 14: \quad & |\boldsymbol{k_m}|^2 = m_1^2 + m_2^2 + m_3^2 + m_4^2 + m_5^2 + m_6^2 + m_7^2 \\
& \qquad + \omega_1(m_1 m_2 + m_2 m_3 + m_3 m_4 + m_4 m_5 + m_5 m_6 + m_6 m_7 - m_7 m_1) \\
& \qquad + \omega_2(m_1 m_3 + m_2 m_4 + m_3 m_5 + m_4 m_6 + m_5 m_7 - m_6 m_1 - m_7 m_2) \\
& \qquad + \omega_3(m_1 m_4 + m_2 m_5 + m_3 m_6 + m_4 m_7 - m_5 m_1 - m_6 m_2 - m_7 m_3)
\end{aligned}
$$

where ω is the golden ratio: $\omega = (1 + \sqrt{5})/2 = 2\cos(\pi/5)$, with $\omega^2 = \omega + 1$, and $\omega_j = 2\cos(j\pi/7)$, with $\omega_2 = \omega_1^2 - 2$ and $\omega_3 = 1 - \omega_1 + \omega_2$. The irrational ω_1 is the root of a cubic equation: $\omega_1^3 - \omega_1^2 - 2\omega_1 + 1 = 0$.

We observe that for $Q = 2$, 4 and 6, $|\boldsymbol{k_m}|^2$ is an integer, so, as expected, points on square and hexagonal lattices cannot come arbitrarily close to the unit circle without actually hitting it.

For $Q = 8$, 10 and 12, $|\boldsymbol{k_m}|^2$ is of the form:

$$|\boldsymbol{k_m}|^2 = 1 + p - rq, \tag{15}$$

where $r = \sqrt{2}$, ω or $\sqrt{3}$ is an irrational root of a quadratic equation with integer coefficients, and p and q are integers. If $p - rq$ is close to zero (that is, if r is well approximated by $\frac{p}{q}$), then $|\boldsymbol{k_m}|^2$ can come close to 1. The particular rational approximations involved are:

	$l=0$	1	2	3	4	5	6	7	8	9	10
$r=\sqrt{2}$	$\frac{p_l}{q_l}=\frac{1}{1}$	$\frac{3}{2}$	$\frac{7}{5}$	$\frac{17}{12}$	$\frac{41}{29}$	$\frac{99}{70}$	$\frac{239}{169}$	$\frac{577}{408}$	$\frac{1393}{985}$	$\frac{3363}{2378}$	$\frac{8119}{5741}$
$r=\omega$	$\frac{p_l}{q_l}=\frac{1}{1}$	$\frac{2}{1}$	$\frac{3}{2}$	$\frac{5}{3}$	$\frac{8}{5}$	$\frac{13}{8}$	$\frac{21}{13}$	$\frac{34}{21}$	$\frac{55}{34}$	$\frac{89}{55}$	$\frac{144}{89}$
$r=\sqrt{3}$	$\frac{p_l}{q_l}=\frac{1}{1}$	$\frac{2}{1}$	$\frac{5}{3}$	$\frac{7}{4}$	$\frac{19}{11}$	$\frac{26}{15}$	$\frac{71}{41}$	$\frac{97}{56}$	$\frac{265}{153}$	$\frac{362}{209}$	$\frac{989}{571}$

Table 1
Continued fraction approximations to $r=\sqrt{2}$, ω and $\sqrt{3}$, as a function of the order l of the truncation.

$$Q=8: \quad \sqrt{2}\approx\frac{p}{q}=\frac{m_1^2+m_2^2+m_3^2+m_4^2-1}{m_4m_1-m_3m_4-m_2m_3-m_1m_2}, \tag{16}$$

$$Q=10: \quad \omega\approx\frac{p}{q}=\frac{m_1^2+\ldots+m_5m_2-1}{m_5m_2-\ldots-m_1m_2}, \tag{17}$$

$$Q=12: \quad \sqrt{3}\approx\frac{p}{q}=\frac{m_1^2+\ldots-m_6m_2-1}{m_6m_1-\ldots-m_1m_2}. \tag{18}$$

In the expressions above, we choose p and q, which depend on the integers $\boldsymbol{m}$, to be positive and to have no common factors.

For $Q=14$ (and higher), $|\boldsymbol{k_m}|^2$ involves the sum of an integer plus integers times at least two different irrationals that will not, in general, be roots of quadratic equations with integer coefficients. Apart from the numerical evidence in figure 4, we do not pursue the cases $Q\geq 14$ further here.

It is clear that the theory of continued fraction approximations of irrationals will be useful here. The continued fraction expressions for the irrationals $r=\sqrt{2}$, ω and $\sqrt{3}$ are (respectively):

$$1+\cfrac{1}{2+\cfrac{1}{2+\cdots}}, \quad 1+\cfrac{1}{1+\cfrac{1}{1+\cdots}}, \quad 1+\cfrac{1}{1+\cfrac{1}{2+\cfrac{1}{1+\cfrac{1}{2+\cdots}}}}. \tag{19}$$

If these fractions are truncated after l terms, the successive fractions p_l/q_l that approximate r are given in table 1. We recall from the theory of continued fractions [36] that

$$\frac{K_1}{q_l^2}<\left|\frac{p_l}{q_l}-r\right|<\frac{K_2}{q_l^2} \tag{20}$$

for $r = \sqrt{2}$, ω, $\sqrt{3}$, and K_1, K_2 are constants. The values of K_1 and K_2, which are order unity, are related to the largest integers appearing in the expansions (19), which are 1 or 2 in these cases. These inequalities mean that the truncated continued fraction expansions $\frac{p_l}{q_l}$ approximate r well, but not too well, as l becomes large. It will also be useful to note that if $l > 1$ and if q is an integer with $0 < q < q_l$, then [36]

$$\left| \frac{p_l}{q_l} - r \right| < \left| \frac{p}{q} - r \right|. \tag{21}$$

This means that if $\frac{p_l}{q_l}$ is the truncation of the continued fraction approximation of an irrational r, no other fraction with a smaller denominator comes closer to r.

If we exclude those vectors $\boldsymbol{k_m}$ that fall exactly on the unit circle, which would have $p = q = 0$, the relations in (20) and (21) can be used to show that $|\boldsymbol{k_m}|^2$ can approach 1 no faster than order N^{-2} for $Q = 8$, 10 and 12. The reason is that the denominators in (16–18) are of the form of a sum of products of the integers $m_1, \ldots, m_{Q/2}$. Since $\sum_j |m_j| = N$, each quadratic term in the denominator can be no larger than N^2 in magnitude; there are no more than Q of these terms, so the denominator as a whole satisfies $q \leq QN^2$. Then, using first (21) and then (20), we have

$$\left| |\boldsymbol{k_m}|^2 - 1 \right| = |p - rq| \geq |p_l - rq_l| > \frac{K_1}{q_l}, \tag{22}$$

where q_l is the smallest of the q_l's above q: $q_{l-1} < q \leq q_l$ (unless $q_{l-1} = q_l = 1$). Now for $r = \sqrt{2}$, ω and $\sqrt{3}$, the q_l's are no further than a factor of 3 apart [36], so $q_l \leq 3q_{l-1} < 3q \leq 3QN^2$, and we have (assuming $|\boldsymbol{k_m}| \neq 1$):

$$\left| |\boldsymbol{k_m}|^2 - 1 \right| > \frac{K}{N^2}, \tag{23}$$

where $|\boldsymbol{m}| = N$ and K is a constant.

We now show that the order N^{-2} rate of approach is indeed achieved for $Q = 8$, 10 and 12. Observe that, for $Q = 8$:

$$\boldsymbol{k_m} = \boldsymbol{k}_1 + p_l \boldsymbol{k}_3 + q_l \boldsymbol{k}_6 + q_l \boldsymbol{k}_8 = (1, p_l - \sqrt{2} q_l), \tag{24}$$

with $|\boldsymbol{m}| = N = p_l + 2q_l + 1$ (even) and $|\boldsymbol{k_m}|^2 - 1 = p_l^2 + 2q_l^2 - 2p_lq_l\sqrt{2}$ (a related vector with $N = 2p_l + 2q_l + 1$ (odd) can also be found); for $Q = 10$:

$$\begin{aligned}\boldsymbol{k_m} &= (p_l + 1)\boldsymbol{k}_2 + (p_l - 1)\boldsymbol{k}_5 + (q_l + 1)\boldsymbol{k}_8 + (q_l - 1)\boldsymbol{k}_9 \\ &= (1, (p_l - \omega q_l)\sqrt{3 - \omega}),\end{aligned} \tag{25}$$

with $|\boldsymbol{m}| = N = 2p_l + 2q_l$ and $|\boldsymbol{k_m}|^2 - 1 = 3p_l^2 + 2q_l^2 + 2p_lq_l - (p_l^2 - q_l^2 + 4p_lq_l)\omega$, using the fact that $\omega^2 = \omega + 1$; and for $Q = 12$:

$$\boldsymbol{k_m} = p_l\boldsymbol{k}_4 + (q_l - 1)\boldsymbol{k}_9 + (q_l + 1)\boldsymbol{k}_{11} = (1, p_l - \sqrt{3}q_l), \tag{26}$$

with $|\boldsymbol{m}| = N = p_l + 2q_l$ and $|\boldsymbol{k_m}|^2 - 1 = p_l^2 + 3q_l^2 - 2p_lq_l\sqrt{3}$. These vectors were found after a prolonged examination of the distances plotted in figure 4.

Using (20), we have, for these particular vectors,

$$\left||\boldsymbol{k_m}|^2 - 1\right| = (p_l - rq_l)^2 \leq \frac{K_2^2}{q_l^2}, \tag{27}$$

where r stands for $\sqrt{2}$, ω or $\sqrt{3}$, with an extra factor of $3-\omega$ in the case $r = \omega$. Using relations like $q_l \leq p_l \leq q_{l+1} \leq 3q_l$ [36], and the relations between N, q_l and p_l above, it is then possible to show in each case that N is less than a constant times q_l, so

$$\left||\boldsymbol{k_m}|^2 - 1\right| < \frac{K'}{N^2}, \tag{28}$$

where K' is a constant. These particular choices of $\boldsymbol{k_m}$ are plotted on the graphs in figure 4(a–c) as stars.

From the graphs it is clear that these particular vectors are not always the closest ones that can be found for given values of N (particularly for $Q = 10$), but they suffice to prove the scaling results required here. If $|\boldsymbol{k_m}|^2 - 1$ as given above (that is, $|\boldsymbol{k_m}|^2 - 1 = p_l^2 + 2q_l^2 - 2p_lq_l\sqrt{2}$ for $Q = 8$, and so on) can be written as $p_{l'} - rq_{l'}$ for some integer l', then we would expect $|\boldsymbol{k_m}|^2$ to be particularly close to 1, compared with other vectors of up to that order. So, for example, an excursion into numerology suggests the following relations, which we have proven for $Q = 8$ by induction: for $Q = 8$, $l' = 2l + 1$; and for $Q = 12$, $l' = 2l + 1$ if l is odd. On the other hand, for $Q = 10$, $p_l^2 - q_l^2 + 4p_lq_l$

does not appear to equal $q_{l'}$ for values of l up to 15, which is probably why the constructed vector does not achieve the closest possible distance in this case.

The summary result of this section is that we have shown that, given an integer N, the vector $\boldsymbol{k_m}$ with $|\boldsymbol{m}| = N$ that comes closest to the unit circle (without being on the unit circle) satisfies

$$\frac{K}{N^2} \leq \left| |\boldsymbol{k_m}|^2 - 1 \right| \leq \frac{K'}{N^2}, \tag{29}$$

for constants K and K', for $Q = 8$, 10 and 12 equally spaced original vectors. The numerical evidence, for $N \leq 10^6$, suggests values for $Q = 8$: $K = 0.72$ and $K' = 16.95$; for $Q = 10$: $K = 0.69$ and $K' = 9.94$; and for $Q = 12$: $K = 0.56$ and $K' = 4.34$.

It should be emphasised that several of the steps in the derivation of these bounds (for example, equation (20)) rely on the fact that $\sqrt{2}$, ω and $\sqrt{3}$ are quadratic irrationals, that is, they are roots of quadratic equations with integer coefficients. This implies that the integers in the continued fraction expansion of these numbers (19) form repeating sequences and so are bounded above. The case of $Q = 14$ (and higher) is more difficult to analyse because the irrational numbers ω_1 and ω_2 in the expression for $|\boldsymbol{k_m}|^2$ in this case are not quadratic irrationals, and because there are two irrationals.

4 The question of convergence

The results of the previous section, taken with (14), imply that when $\boldsymbol{k_m}$ is close to the unit circle, $\mathcal{L}_0^{-1}(e^{i\boldsymbol{k_m}\cdot\boldsymbol{x}})$ can be as large as a constant times $N^4 e^{i\boldsymbol{k_m}\cdot\boldsymbol{x}}$ for $Q = 8$, 10 and 12, with $N = |\boldsymbol{m}|$.

At each stage in the calculation, the linear operator $\mathcal{L}_0$ is inverted as in (13):

$$U_n = \mathcal{L}_0^{-1}\left(-\mathcal{N}_n(U_1, \ldots, U_{n-1})\right), \tag{30}$$

where we simplify the discussion by dropping the parameter and the time dependence, and we assume that the solvability condition has been satisfied so that $\mathcal{L}_0$ can be inverted . The nonlinear terms $\mathcal{N}_n$ will contain modes $e^{i\boldsymbol{k_m}\cdot\boldsymbol{x}}$ with $|\boldsymbol{m}|$ up to and including n, so, at least at first glance, U_n will be n^4 times

larger than the product of various combinations of $U_1, \ldots, U_{n-1}$. In particular, the combination $U_1 U_{n-1}$ occurs in $\mathcal{N}_n$. This suggests that U_n is n^4 times larger than U_{n-1}, which is $(n-1)^4$ times larger than U_{n-2}, and so on – so U_n will be of order $(n!)^4$. The perturbation method should yield the pattern $U(x,y)$ as the limit:

$$U = \lim_{N\to\infty} \sum_{n=1}^{N} \epsilon^n U_n, \tag{31}$$

but if U_n is as large as $(n!)^4$, the limit will not converge for nonzero ϵ. For the limit to converge, U_n should be no larger than a constant raised to the power of n.

In fact, the $(n!)^4$ estimate is unduly pessimistic, since there will be cancellations. Moreover, if we focus on nonlinear interactions in $\mathcal{N}_n$ that result in modes with wavevectors on the unit circle, the modes that are close to the unit circle involved in these nonlinear interactions will originate from $U_{n/2}$, not from U_{n-1}. The reason is that the terms in $\mathcal{N}_n$ involve products like $U_1 U_{n-1}$, $U_2 U_{n-2}$, $\ldots$, $U_{n/2}^2$. Now the term $U_1 U_{n-1}$ cannot generate modes closer to the unit circle than the modes already in U_{n-1}. Modes that are closer than any previous combination will come (if at all) from combinations like $U_{n/2}^2$, and will involve the modes in $U_{n/2}$ that are close to the unit circle. This leads to an estimate of the form: U_n will be n^4 times larger than $U_{n/2}^2$, which will be $(n/2)^8$ times larger than $U_{n/4}^4$, and so on. The resulting estimate for U_n will not be as large as $(n!)^4$, but it will still be larger than any constant raised to the power of n.

Unfortunately, it is difficult to be more precise than this, but the arguments above certainly cast doubt on the convergence of the modified perturbation theory method as applied in this way to determine the amplitude of a quasi-pattern as a function of parameter. At best the series will be *asymptotic*, that is, not converging and yet still yielding useful information when truncated at low order.

As a cautionary tale, we turn briefly to the asymptotic series representation of the Stieltjes integral, as described in [37]:

$$I = \int_0^\infty \frac{e^{-t}}{1+\epsilon t}\, dt = \int_0^\infty \left\{1 - \epsilon t + \epsilon^2 t^2 - \ldots\right\} e^{-t}\, dt = \sum_{n=0}^{\infty} (-1)^n n! \epsilon^n. \tag{32}$$

I is a perfectly well defined integral, depending on a small positive parameter ϵ. The fraction may be expanded formally as a power series in ϵ, but this step is invalid, as the sum does not converge if $t > 1/\epsilon$, and the upper limit of the integral is $t =$ infinity. The formal power series can be integrated term by term, resulting in an infinite sum for the value of I as a function of ϵ. This sum does not converge for any nonzero ϵ, and yet, if the sum is truncated at a fixed order N, then there is a range of ϵ for which the truncated sum gives a reasonable approximation of I [37]. Taking a larger N results in a smaller range of ϵ, closer to zero. On the other hand, if ϵ is fixed at a small number, then there is a a truncation N that gives an estimate of I that is reasonably close to the correct value. The truncation can be increased as ϵ is taken to be smaller.

The danger is that the relation between the usable range of ϵ and the level of truncation is not known in advance. The most severe truncation ($I = 1$) is the safest, but loses useful information about the dependence of I on ϵ.

In the next section, we take the specific example of steady quasipattern solutions of the cubic Swift–Hohenberg equation (6). The equivalent severe truncation would have the amplitude of the quasipattern be $\sqrt{\mu}$, which has been widely used by authors who are relying on the small divisor problem alluded to above not rendering this truncation meaningless.

5 Example: the Swift–Hohenberg equation

In this section, we go through the details of deriving expressions for the amplitudes in the specific example of steady solutions of the Swift–Hohenberg equation (6). This is one of the simplest pattern-forming PDEs, and serves to illustrate the problem at hand.

For this presentation, we concentrate on the case $Q = 2$, but we have carried out the computations for $Q = 2, \ldots, 12$ and up to 33^{rd} order in ϵ. The symmetry $U \to -U$ implies that all even terms U_2, U_4, etc., are absent, that $\mu_1 = 0$, and that time should be scaled by ϵ^{-2}. To simplify the presentation, we will only seek steady solutions, and so drop the time derivative terms. By taking ϵ^2 to be the bifurcation parameter, we can set $\mu_2 = 1$ (taking μ_2 to be positive

since the bifurcation is supercritical). The expansion is then

$$U = \epsilon U_1 + \epsilon^3 U_3 + \epsilon^5 U_5 + \ldots, \qquad \mu = \epsilon^2, \tag{33}$$

with $\mathcal{L}_0(U) = -(1+\nabla^2)^2 U$.

The leading order equation at order ϵ is $\mathcal{L}_0(U_1) = 0$, which is solved by (for real U and with $Q = 2$ modes, for clarity of exposition):

$$U_1(x,y) = A_1 e^{ix} + \bar{A}_1 e^{-ix}, \tag{34}$$

where altering the phase of the complex amplitude A_1 translates the pattern.

At third order in ϵ, the equation we have to solve is:

$$\mathcal{L}_0(U_3) = -U_1 + U_1^3. \tag{35}$$

Now $U_1^3 = A_1^3 e^{3ix} + 3|A_1|^2 A_1 e^{ix} + \text{c.c.}$ (where c.c. stands for complex conjugate), and since $\mathcal{L}_0(U_3)$ cannot contain e^{ix} and e^{-ix}, equation (35) gives:

$$0 = A_1 - 3|A_1|^2 A_1. \tag{36}$$

This equation would usually have a factor of μ_2 in front of the linear term, but we have set this to 1. The nontrivial solution of this equation is $A_1 = 1/\sqrt{3}$, where we may take A_1 to be real without loss of generality. The operator $\mathcal{L}_0$ acts on a mode $e^{i\boldsymbol{k}\cdot\boldsymbol{x}}$ as $\mathcal{L}_0(e^{i\boldsymbol{k}\cdot\boldsymbol{x}}) = -(1-k^2)^2 e^{i\boldsymbol{k}\cdot\boldsymbol{x}}$, so $\mathcal{L}_0(U_3)$ can be inverted to give:

$$U_3 = -\frac{1}{192\sqrt{3}}\left(e^{3ix} + e^{-3ix}\right) + A_3 e^{ix} + \bar{A}_3 e^{-ix}, \tag{37}$$

where we have included an arbitrary combination of the original modes on the unit circle (in the kernel of $\mathcal{L}_0$), which will allow the solvability condition to be satisfied at the next order.

At fifth order in ϵ, the equation we have to solve is:

$$\begin{aligned} \mathcal{L}_0(U_5) &= -U_3 + 3U_1^2 U_3 \\ &= -\frac{1}{192\sqrt{3}}\left(e^{ix} + e^{3ix} + e^{5ix}\right) + A_3 e^{3ix} + (A_3 + \bar{A}_3)e^{ix} + \text{c.c.} \end{aligned} \tag{38}$$

	$Q=2$	4	6	8	10	12
A_3	$10^{-2.11}$	$10^{-0.72}$	$10^{0.57}$	$10^{0.78}$	$10^{1.11}$	$10^{1.54}$
A_5	$-10^{-3.40}$	$-10^{-0.95}$	$-10^{1.26}$	$-10^{2.37}$	$-10^{3.08}$	$-10^{3.86}$
A_7	$10^{-5.61}$	$-10^{-2.67}$	$-10^{2.75}$	$10^{4.75}$	$10^{6.21}$	$10^{7.15}$
A_9	$10^{-5.91}$	$10^{-1.17}$	$10^{3.70}$	$-10^{7.22}$	$-10^{9.58}$	$-10^{10.79}$
A_{11}	$-10^{-7.16}$	$-10^{-1.36}$	$10^{5.30}$	$10^{9.97}$	$10^{12.95}$	$10^{14.40}$
A_{13}	$-10^{-8.62}$	$-10^{-1.57}$	$-10^{6.30}$	$-10^{12.88}$	$-10^{16.31}$	$-10^{17.98}$
A_{15}	$10^{-9.31}$	$10^{-1.22}$	$-10^{7.94}$	$10^{15.79}$	$10^{19.66}$	$10^{21.55}$
A_{17}	$-10^{-10.90}$	$-10^{-1.75}$	$10^{8.96}$	$-10^{18.71}$	$-10^{23.01}$	$-10^{25.14}$
A_{19}	$-10^{-11.65}$	$-10^{-1.31}$	$10^{10.64}$	$10^{21.61}$	$10^{26.34}$	$10^{28.74}$
A_{21}	$10^{-12.70}$	$10^{-1.24}$	$-10^{11.65}$	$-10^{24.52}$	$-10^{29.68}$	$-10^{32.38}$
A_{23}	$10^{-14.47}$	$10^{-1.96}$	$-10^{13.37}$	$10^{27.46}$	$10^{33.02}$	$10^{36.07}$
A_{25}	$-10^{-14.83}$	$-10^{-1.13}$	$10^{14.37}$	$-10^{30.48}$	$-10^{36.36}$	$-10^{39.80}$
A_{27}	$10^{-16.22}$	$10^{-1.34}$	$10^{16.12}$	$10^{33.64}$	$10^{39.71}$	$10^{43.57}$
A_{29}	$10^{-17.18}$	$10^{-1.29}$	$-10^{17.10}$	$-10^{36.93}$	$-10^{43.07}$	$-10^{47.35}$
A_{31}	$-10^{-18.10}$	$-10^{-1.01}$	$-10^{18.88}$	$10^{40.29}$	$10^{46.46}$	$10^{51.15}$

Table 2
Values of the coefficients A_n in (39). These data are also plotted in figure 5.

The solvability condition can be satisfied by setting $A_3 = 1/384\sqrt{3}$, with an arbitrary imaginary component (set to zero) that corresponds to a small translation of the original pattern. With the e^{ix} component removed, $\mathcal{L}_0$ can be inverted to give U_5.

This procedure is repeated up to some order N, resulting in a power series for the original pattern U:

$$U = \left(\frac{\epsilon}{\sqrt{3}} + \frac{1}{128}\left(\frac{\epsilon}{\sqrt{3}}\right)^3 - \frac{13}{32768}\left(\frac{\epsilon}{\sqrt{3}}\right)^5 + \ldots\right)\left(e^{ix} + e^{-ix}\right) + \left(-\frac{1}{64}\left(\frac{\epsilon}{\sqrt{3}}\right)^3 + \frac{3}{8192}\left(\frac{\epsilon}{\sqrt{3}}\right)^5 + \ldots\right)\left(e^{3ix} + e^{-3ix}\right) + \ldots$$

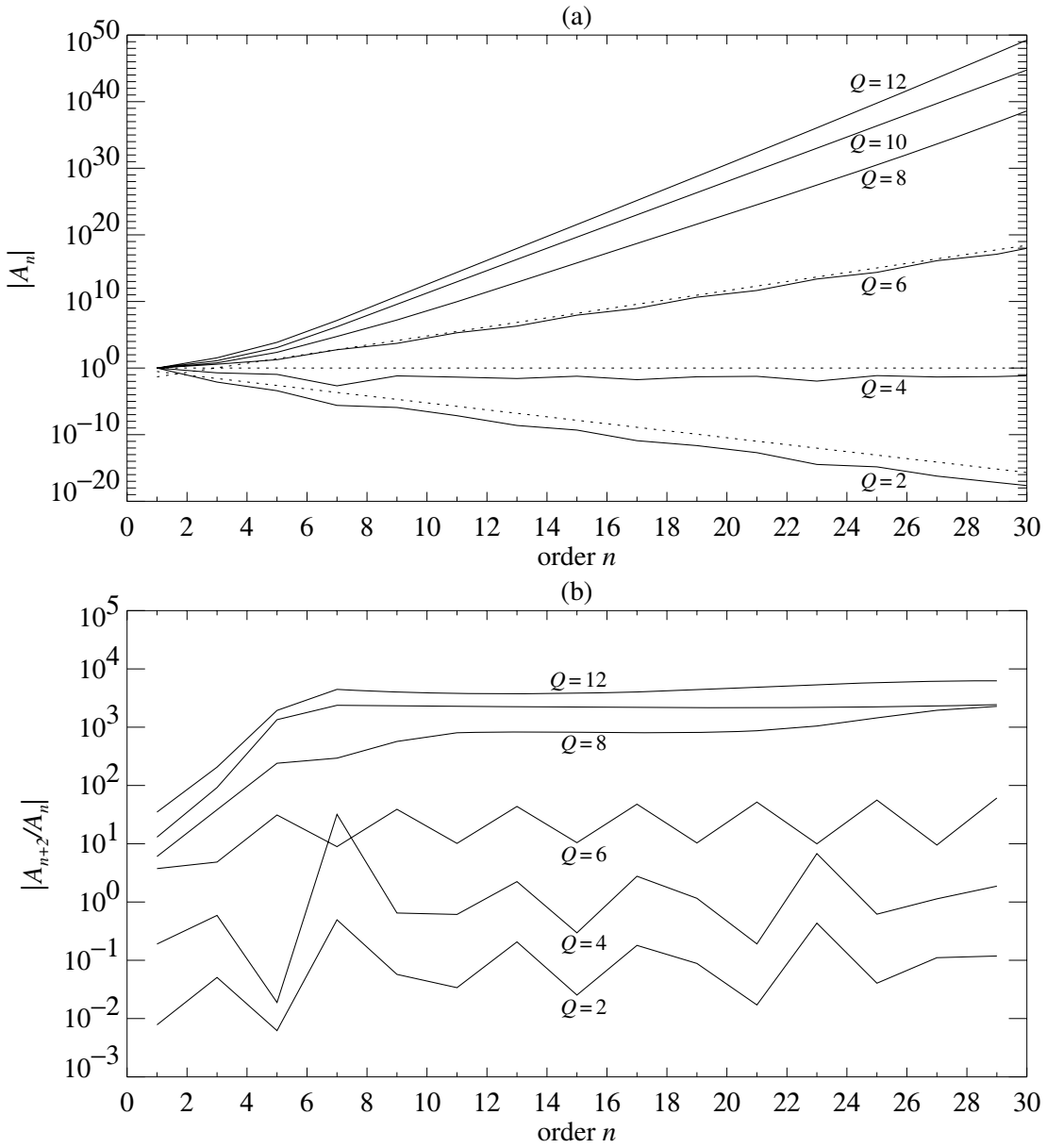

Fig. 5. (a) Absolute values of the coefficients A_n in (39) for $Q = 2$ (lowest line), 4, 6, 8, 10 and 12 (top line) modes. These data are also given in table 2. Straight lines indicate that the coefficient of the modes on the unit circle will converge as the order of truncation N is increased, and the inverse of the slope of the straight line gives the radius of convergence. The dotted lines are 0.3^n (lowest), 1^n and 4.8^n (highest). (b) Ratios A_{n+2}/A_n against n: this ratio continues to increase with n for $Q \geq 8$, indicating that the sum in (40) may not converge for nonzero ϵ.

$$+\left(\frac{1}{12288}\left(\frac{\epsilon}{\sqrt{3}}\right)^5+\ldots\right)\left(e^{5ix}+e^{-5ix}\right)+\ldots$$
$$=\left(\sum_{n=1,3,\ldots}^{N}A_n\left(\frac{\epsilon}{\sqrt{3}}\right)^n\right)\left(e^{ix}+e^{-ix}\right)+\ldots \qquad (39)$$

where A_n is the coefficient of $(\epsilon/\sqrt{3})^n$ in the expression for the amplitude of the modes on the unit circle. The factor $\sqrt{3}$ is chosen so that $A_1 = 1$ (so the A_1 and A_3 here are rescaled from the A_1 and A_3 above). The calculation can be carried out for other values of Q; for $Q = 4, 6, \ldots, 12$, the scaling for amplitudes is $\sqrt{9}, \sqrt{15}, \ldots, \sqrt{33}$, so $A_1 = 1$ in all cases. The values of the first few coefficients A_n are given in table 2 and plotted in figure 5.

In these calculations, all modes generated by nonlinear interactions were kept for $Q = 2$, 4 and 6. For the other three cases, we kept only modes with wavenumbers up to $\sqrt{5}$, to keep the total number of modes within manageable limits. Even so, with $Q = 12$, there were more than 15000 modes generated at the highest order – without this truncation, there would have been almost 2 million. We checked the lower orders against calculations keeping all modes, and the differences in the mode amplitudes were about 1%. Restricting the number of modes in this way had no effect on how close combinations of wavevectors could get to the unit circle.

For $Q = 2$, 4 and 6, it appears that there will be no problem with the convergence of the coefficient of the modes on the unit circle in (39) since the coefficients A_n grow no faster than a constant to the power of n (indicated by straight dotted lines in figure 5a). The bound on the ratios A_{n+2}/A_n also indicates the range of values of ϵ for which convergence is expected.

For $Q = 8$, 10 and 12, the situation is less clear. The values of the coefficients in table 2 are certainly very large (10^{50}), but they are multiplied by the small parameter ϵ raised to high powers. At first glance, the values of the coefficients in figure 5(a) appear to be going up as straight lines (which would indicate convergence), but the ratios A_{n+2}/A_n in figure 5(b) show that the slopes of these lines plateau for n in the range 12–18, and then start to increase gradually for larger n, suggesting that the coefficients A_n are growing faster than a constant raised to the power of n, and casting doubt on the convergence of (39) as the level of truncation is increased.

The fact that the ratios A_{n+2}/A_n plateau and then start climbing in figure 5(b) can be related to the nonlinear interaction of modes at each order in the perturbation theory. Taking $Q = 8$ to be specific, for $7 \leq n \leq 9$ and for $11 \leq n \leq 17$, the values of $|\boldsymbol{k_m}|^2$ generated up to these orders, closest to the unit circle, are 0.85786 and 1.05887 respectively. Even though these modes close to the unit circle are generated at some order n, they do not influence the value of the coefficient of modes on the unit circle until nonlinear interactions work their way back: this will occur at order $2n+1$. As a result, we expect the jump in k^2 from $n = 9$ to 11 to influence A_{23} – indeed, the ratios start to climb at A_{23}, and more sharply at A_{25}. We would then expect these ratios to plateau and then start climbing at order 39, plateau and climb again as wavevectors generated at higher order come closer to the unit circle. The same reasoning would predict the ratios to start climbing at $n = 27$ for $Q = 10$ and at $n = 15$ and 23 for $Q = 12$, at least roughly consistent with the data in figure 5(b). It was only by going to such high order that these issues became clear.

Equation (39) can be used to find the amplitude $A^{(N)}$ of modes on the unit circle as a function of the original parameter $\mu = \epsilon^2$ when the expression is truncated to include powers in ϵ up to and including ϵ^N:

$$A^{(N)} = \sqrt{\mu} \sum_{n=1,3,\ldots}^{N} A_n \mu^{(n-1)/2}, \tag{40}$$

where the amplitude has been rescaled (as indicated above) so that $A^{(1)} = \sqrt{\mu}$ for all values of Q. Graphs of $A^{(N)}$ as functions of μ for $N = 1$ to 31 and for $Q = 2$ to 12 are presented in figures 6 and 7. For $Q = 2$, 4 and 6 (figure 6a–c and figure 7a), the curves of $A^{(N)}$ against μ converge as N increases in a manner consistent with the straight line increases of A_n in figure 5(a). In fact, an estimate of the radius of convergence can be made from the slopes: the series will converge for $\mu \leq 32$ for $Q = 2$, $\mu \leq 9$ for $Q = 4$, and $\mu \leq 0.65$ for $Q = 6$. These limits are roughly half the values of μ at which modes generated in nonlinear interactions become linearly unstable.

On the other hand, for $Q \geq 8$ (figure 6d–f and figure 7b–d), at each level of truncation N, the graph of $A^{(N)}$ against μ diverges at a value of μ that is decreases as N becomes larger, consistent with the steady increase in the ratio A_{n+2}/A_n as n increases. Indeed, modes generated in nonlinear interactions become linearly unstable for μ arbitrarily close to zero, for large enough N.

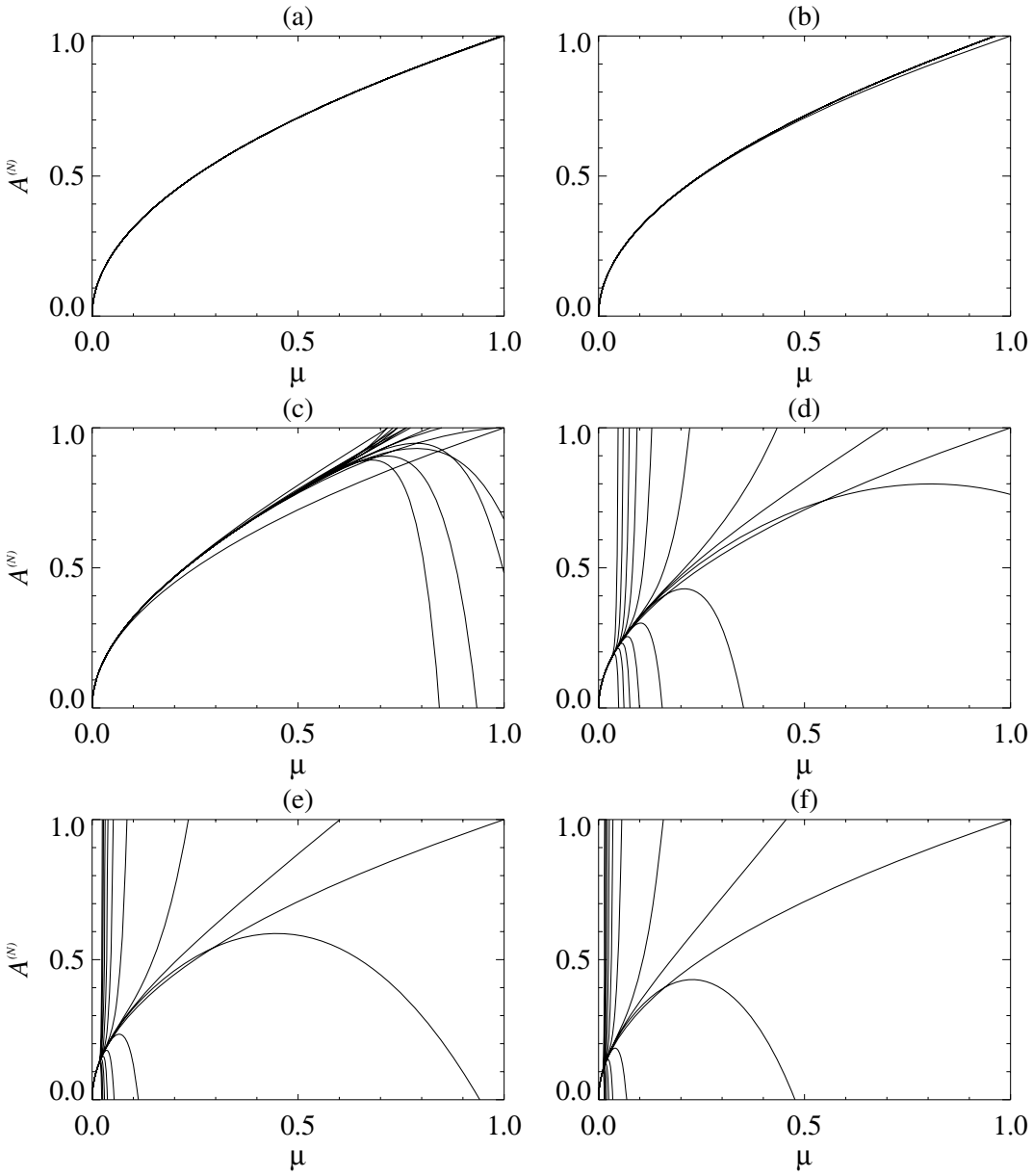

Fig. 6. Scaled amplitude $A^{(N)}$ as a function of μ from (40), for (a) $Q = 2$, (b) $Q = 4$, (c) $Q = 6$, (d) $Q = 8$, (e) $Q = 10$, (f) $Q = 12$, for different levels of truncation $N = 1, \ldots, 31$. For $Q = 2$ and $Q = 4$, increasing the order of truncation has little effect for μ up to 1, while for $Q = 6$, it appears that increasing the order of truncation converges to a solution only for $\mu < 0.65$ or so. However, for $Q \geq 8$, increasing the order of truncation leads to graphs of $A^{(N)}$ as a function of μ that appear to diverge for μ closer and closer to zero as N becomes larger. Details of (c–f) are shown in figure 7.

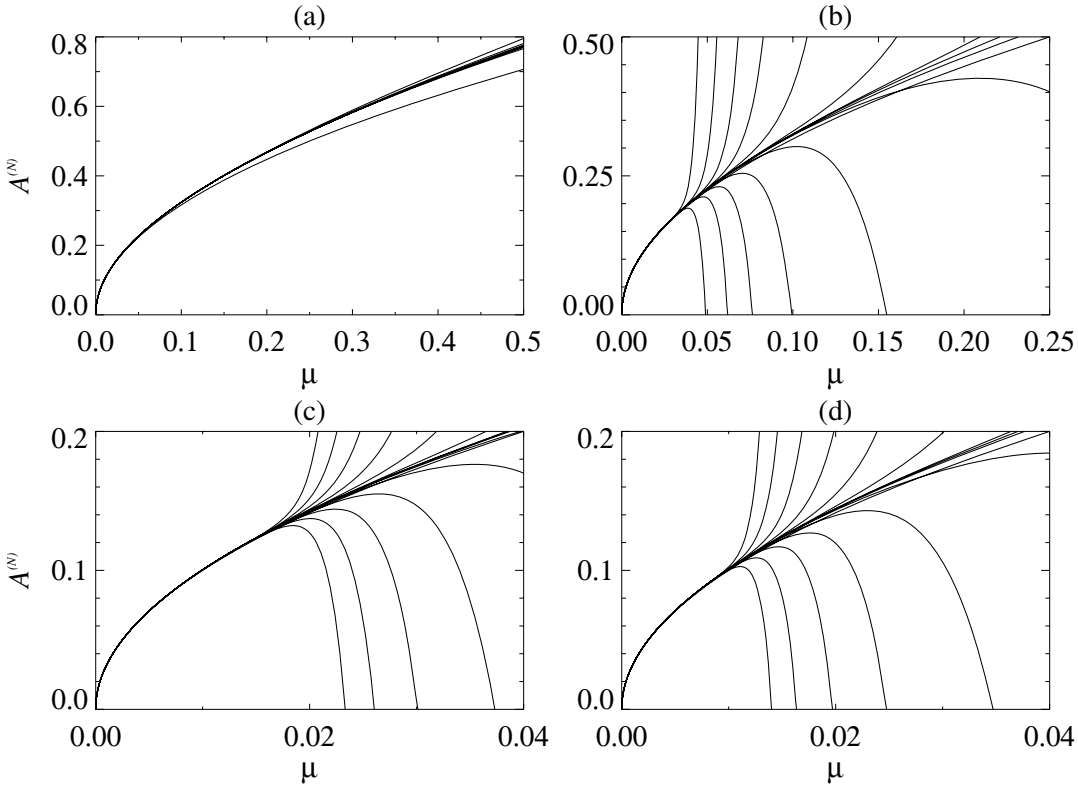

Fig. 7. Detail of figure 6, for (a) $Q = 6$, (b) $Q = 8$, (c) $Q = 10$, (d) $Q = 12$. Note how for $Q \geq 8$, there is no sign that the graphs of $A^{(N)}$ against μ are settling down as N increases.

However, it appears from these graphs that for μ sufficiently small (say, less than 0.01 for $Q = 8$), there is a chance of convergence. Without proper estimates of the rate of increase of A_n with n, it is impossible to know for certain whether or not this method converges, and if it does not, whether or not the truncated estimates converge to the true solution (if it exists) in the limit of small ϵ.

6 Discussion

In summary, we have shown that modes generated by nonlinear interactions between $Q = 8$, 10 and 12 Fourier modes with wavevectors equally spaced around the unit circle have wavevectors that can approach the unit circle no faster than a constant times n^{-2}, where n is the number of modes involved. We have also shown by construction that there are combinations of modes that do achieve this limit.

When carrying out modified perturbation theory in order to compute the amplitude of a pattern as a function of a parameter, the usual approach is to start with two assumptions: first, that when the parameter is small, the desired pattern U can be written as a power series in that small parameter; and second, the primary modes of interest have wavevectors equally distributed around the unit circle. At each order n in the theory, nonlinear terms generate modes involving up to n of the Q modes. The modes that fall exactly on the unit circle are dealt with by applying a solvability condition, while equations for modes off the unit circle are satisfied by inverting the linear operator $\mathcal{L}_0$. In the cases $Q = 2$, 4 and 6, the patterns are spatially periodic and modes generated by nonlinear interactions do not approach the unit circle. For $Q = 8$, 10 and 12, the wavevector can come within n^{-2} of the unit circle, and small divisors (order n^{-4}) appear when inverting $\mathcal{L}_0$, leading to numerically large coefficients in front of the Fourier modes. These coefficients grow sufficiently rapidly with n that convergence of the power series for the pattern U is called into question.

We have explicitly carried out modified perturbation theory up to 33^{rd} order for the cubic Swift–Hohenberg equation. Of course, this kind of calculation cannot demonstrate convergence or otherwise, but it does illustrate the issues that arise. The main conclusion of the calculation is that even if modified perturbation theory does generate a convergent series approximation to the quasipattern for small enough μ, the series certainly diverges if the parameter μ is bigger than about 0.01, depending on exactly which value of Q is used. It might be possible that the series do converge for smaller μ, though we have argued that this is not the case. Even if the series do diverge for all nonzero μ, a low-order truncation may still give a useful approximation of the quasipattern, assuming that the equations do have a quasipattern solution. It is on this basis that other researchers have proceeded.

There are two related issues at stake. First, existence: do pattern forming PDEs like the 2-dimensional Swift–Hohenberg equation have quasipattern solutions that bifurcate from the trivial solution? Second, given the small divisor problem, can asymptotic methods like modified perturbation theory yield useful approximations to these solutions? We have not addressed the first issue in this paper, but plan to turn to it in future. The limits we have derived on the rate of approach of wavevectors to the unit circle will play a central role in that calculation. As for the second issue, we have shown that modi-

fied perturbation theory does not converge sufficiently rapidly (or slowly) to provide an answer unequivocally one way or the other, and so this standard method should not be regarded as a reliable way of computing properties of quasipatterns.

What is needed is a method that converges more rapidly. Each order in the standard theory gains a factor of ϵ as well as large factors from any small divisors that arise. There are other methods, developed for proofs of KAM theory (see [32]) that converge more rapidly, and these may be required for a rigorous treatment of quasipatterns as well. The difference between the KAM situation and that of quasipatterns is that in the KAM case, the solutions of interest are quasiperiodic in only one dimension (time), while in the second, quasipatterns are quasiperiodic in two space directions.

By making arbitrarily small perturbations to the Q wavevectors, it is possible to make qualitative alterations to the nature of the problem in the cases $Q = 8$, 10 and 12. For instance, the patterns can be made periodic on square or hexagonal lattices, with a lower limit to how close vectors can get to the unit circle. For example, in the case $Q = 12$, choosing the modes $(1, 0)$, $(\frac{2p_lq_l}{p_l^2+q_l^2}, \frac{p_l^2-q_l^2}{p_l^2+q_l^2})$ and so on. where $\frac{p_l}{q_l}$ is a continued fraction approximation to $\sqrt{3}$ (see table 1) yields 12 modes on the unit circle that become nearly equally spaced as l increases, and that generate a square lattice by virtue of $(p_l^2 - q_l^2, 2p_lq_l, p_l^2 + q_l^2)$ being Pythagorean triplets – see [38] for more details. Similarly, 12-dimensional representations of the group $D_6 \ltimes T^2$ can be chosen so that the modes are nearly equally spaced and yet they generate a hexagonal lattice [19]. Even in a square periodic domain, approximate $Q = 12$ quasipatterns can be generated [24]. The 8-dimensional representations of $D_4 \ltimes T^2$ can be used to approximate 8-fold quasipatterns in the same way, though it is not clear how a 10-fold quasipattern could be approximated by a periodic pattern. The drawback with approximating quasipatterns by periodic patterns in these ways is that the range of validity of the normal forms derived shrinks to zero as the approximation improves.

It is interesting to note that 8, 10 and 12-fold quasipatterns have been observed experimentally for several years now, but no 14-fold (or higher) quasipattern has been reported (cf. [23]), with the possible exception of [14]. One might speculate that the reason for this is that the convergence issues discussed above are likely to be more serious in the case $Q = 14$ since wavevectors

approach the unit circle much more rapidly than in the cases 8, 10 and 12 (see figure 4).

Acknowledgements

We are grateful to many people who have helped shape these ideas, in one way or another, over a period of several years: Peter Ashwin, Jon Dawes, Jay Fineberg, Rebecca Hoyle, Edgar Knobloch, Paul Matthews, Ian Melbourne, Michael Proctor, Hermann Riecke and Mary Silber. The research of AMR is supported by the Engineering and Physical Sciences Research Council.

References

[1] M.C. Cross and P.C. Hohenberg, Pattern formation outside of equilibrium, *Rev. Mod. Phys.* **65** (1993) 851–1112.

[2] M.I. Rabinovich, A.B. Ezersky and P.D. Weidman, *The Dynamics of Patterns* (World Scientific, Singapore, 2000).

[3] H. Arbell and J. Fineberg, Pattern formation in two-frequency forced parametric waves, *Phys. Rev. E* **65** (2002) 036224.

[4] M. Golubitsky, I. Stewart and D.G. Schaeffer, *Singularities and Groups in Bifurcation Theory. Volume II* (Springer, New York, 1988).

[5] J. Carr, *Applications of Centre Manifold Theory* (Springer, New York, 1981).

[6] C. Janot, *Quasicrystals: a Primer, 2nd edition* (Clarendon Press, Oxford, 1994).

[7] B. Christiansen, P. Alstrøm and M.T. Levinsen, Ordered capillary-wave states: quasicrystals, hexagons and radial waves, *Phys. Rev. Lett.* **68** (1992) 2157–2160.

[8] W.S. Edwards and S. Fauve, Parametrically excited quasicrystalline surface waves, *Phys. Rev. E* **47** (1993) R788–R791.

[9] W.S. Edwards and S. Fauve, Patterns and quasi-patterns in the Faraday experiment, *J. Fluid Mech.* **278** (1994) 123–148.

[10] A. Kudrolli, B. Pier and J.P. Gollub, Superlattice patterns in surface waves, *Physica* **123D** (1998) 99–111.

[11] D. Binks and W. van de Water, Nonlinear pattern formation of Faraday waves, *Phys. Rev. Lett.* **78** (1997) 4043–4046.

[12] D. Binks, M.-T. Westra and W. van de Water, Effect of depth on the pattern formation of Faraday waves, *Phys. Rev. Lett.* **79** (1997) 5010–5013.

[13] H.W. Müller, R. Friedrich and D. Papathanassiou, Theoretical and experimental investigations of the Faraday instability, in: F.H. Busse and S.C. Müller, eds., *Evolution of Spontaneous Structures in Dissipative Continuous Systems* (Springer, Berlin, 1998) 230–265.

[14] E. Pamploni, P.L. Ramazza, S. Residori and F.T. Arecchi, Two-dimensional crystals and quasicrystals in nonlinear optics, *Phys. Rev. Lett.* **74** (1995) 258–261.

[15] S. Longhi, Transverse patterns in nondegenerate intracavity second-harmonic generation, *Phys. Rev. A* **59** (1999) 4021–4040.

[16] W. Zhang and J.Viñals, Square patterns and quasipatterns in weakly damped Faraday waves, *Phys. Rev. E* **53** (1996) R4283–R4286.

[17] H.W. Müller, Model equations for two-dimensional quasipatterns, *Phys. Rev. E* **49** (1994) 1273–1277.

[18] R. Lifshitz and D.M. Petrich, Theoretical model for Faraday waves with multiple-frequency forcing, *Phys. Rev. Lett.* **79** (1997) 1261–1264.

[19] M. Silber, C.M. Topaz and A.C. Skeldon, Two-frequency forced Faraday waves: weakly damped modes and patterns selection, *Physica* **143D** (2000) 205–225.

[20] C.M. Topaz and M. Silber, Resonances and superlattices pattern stabilization in two-frequency forced Faraday waves, *Physica* **172D** (2002) 1–29.

[21] J. Porter and M. Silber, Broken symmetries and pattern formation in two-frequency forced Faraday waves, *Phys. Rev. Lett.* **89** (2002) 084501.

[22] B.A. Malomed, A.A. Nepomnyashchiĭ and M.I. Tribelskiĭ, Two-dimensional quasiperiodic structures in nonequilibrium systems, *Sov. Phys. JETP* **69** (1989) 388–396.

[23] A.C. Newell and Y. Pomeau, Turbulent crystals in macroscopic systems, *J. Phys. A* **26** (1993) L429–L434.

[24] H.G. Solari and G.B. Mindlin, Quasicrystals and strong interactions between square modes, *Phys. Rev. E* **56** (1997) 1853–1858.

[25] B. Echebarria and H. Riecke, Sideband instabilities and defects of quasipatterns, *Physica* **158D** (2001) 45–68.

[26] L.M. Pismen, Bifurcation into wave patterns and turbulence in reaction-diffusion equations, *Phys. Rev. A* **23** (1981) 334–344.

[27] A.A. Golovin, A.A. Nepomnyashchy and L.M. Pismen, Pattern formation in large-scale Marangoni convection with deformable interface, *Physica* **81D** (1995) 117–147.

[28] P. Lyngshansen and P. Alstrøm, Perturbation theory of parametrically driven capillary waves at low viscosity, *J. Fluid Mech.* **351** (1997) 301–344.

[29] P. Chen and J.Viñals, Amplitude equation and pattern selection in Faraday waves, *Phys. Rev. E* **60** (1999) 559–570.

[30] W.V.R. Malkus and G. Veronis, Finite amplitude cellular convection, *J. Fluid Mech.* **4** (1958) 225–260.

[31] A. Schlüter, D. Lortz and F. Busse, On the stability of steady finite amplitude convection, *J. Fluid Mech.* **23** (1965) 129–144.

[32] J. Moser, *Stable and Random Motions in Dynamical Systems* (Princeton University Press, Princeton, 1973).

[33] G. Iooss and J. Los, Bifurcation of spatially quasi-periodic solutions in hydrodynamic stability problems, *Nonlinearity* **3** (1990) 851–871.

[34] J. Swift and P.C. Hohenberg, Hydrodynamic fluctuations at the convective instability, *Phys. Rev. A* **15** (1977) 319–328.

[35] I. Melbourne, Steady-state bifurcation with Euclidean symmetry, *Trans. Am. Math. Soc.* **351** (1999) 1575–1603.

[36] G.H. Hardy and E.M. Wright, *An Introduction to the Theory of Numbers, 4th edition* (Clarendon Press, Oxford, 1960).

[37] C.M. Bender and S.A. Orszag, *Advanced Mathematical Methods for Scientists and Engineers* (McGraw–Hill, New York, 1978).

[38] J.H.P. Dawes, P.C. Matthews and A,M. Rucklidge, Reducible actions of $D_4 \ltimes T^2$: superlattice patterns and hidden symmetries, Submitted to *Nonlinearity* (2003).

A Appendix: method for finding the closest modes

In this appendix, we present an order N^2 algorithm for finding which combinations of up to N vectors end up near the unit circle. The method is suitable for $Q = 8$, 10 and 12, and can be extended to an order N^4 method for $Q = 14$. We focus on $Q = 12$ for definiteness, and let $\boldsymbol{k}_1 = (1, 0)$, $\boldsymbol{k}_2 = (\cos(2\pi/12), \sin(2\pi/12))$, etc.

For each value of N, we want to find non-negative integers m_j ($j = 1, \ldots, 12$) such that $\boldsymbol{k}_{\boldsymbol{m}} = \sum_j m_j \boldsymbol{k}_j$ is close to the unit circle, with $|\boldsymbol{m}| = \sum_j |m_j| = N$, and $\boldsymbol{m}$ achieves this minimum distance to the unit circle for this N. In fact, we are interested in all combinations with $|\boldsymbol{m}| \leq N$ satisfying this minimality condition. The requirement of minimality and the symmetries of the problem lead to restrictions on the integers m_j that allow the order N^2 algorithm

By rotating the vectors, we may choose $m_1 > 0$, without loss of generality.

The requirement for minimality amounts to considering only those m_j where there is no set of values m'_j such that $\sum_j m_j \boldsymbol{k}_j = \sum_j m'_j \boldsymbol{k}_j$ and $\sum |m'_j| < \sum |m_j|$. Using mod 12 arithmetic, this leads to:

- If $m_j > 0$ then $m_{j+6} = 0$, since otherwise let $m'_j = m_j - m_{j+6}$ and $m'_{j+6} = 0$ (or the other way round if $m_{j+6} > m_j$), with $m'_l = m_l$ for $l \neq j$, $j + 6$. This gives a smaller set of vectors summing to the same point.
- If $m_j > 0$ then $m_{j+4} = 0$, since $\boldsymbol{k}_j + \boldsymbol{k}_{j+4} = \boldsymbol{k}_{j+2}$, and we can let: $m'_{j+2} = m_{j+2} + \min(m_j, m_{j+4})$ $m'_j = m_j - \min(m_j, m_{j+4})$ $m'_{j+4} = m_{j+4} - \min(m_j, m_{j+4})$ $m'_l = m_l$ for $l \neq j$, $j + 2$, $j + 4$.
- Similarly, if $m_j > 0$ then $m_{j+8} = 0$.

Combined with $m_1 > 0$, these imply $m_5 = m_7 = m_9 = 0$. Also, only one of m_3 and m_{11} can be nonzero, by the same arguments. Using mirror symmetry, choose $m_3 > 0$ and $m_{11} = 0$.

Similar arguments applied to m_2, m_4, m_6, m_8, m_{10} and m_{12} imply that only two of these can be nonzero, and those two must be separated by 2: m_2 and m_4, or m_4 and m_6, or m_6 and m_8, or m_8 and m_{10}, or m_{10} and m_{12}, or m_{12} and m_2. Consider these in turn, with $m_1 > 0$ and $m_3 > 0$.

- $m_2 > 0$ and $m_4 > 0$: if these two are nonzero, then all possible values of

$\boldsymbol{k_m} = \sum_j m_j \boldsymbol{k}_j$ are in the upper right quadrant and cannot be close to the unit circle.

- $m_4 > 0$ and $m_6 > 0$: all possible values of $\boldsymbol{k_m}$ lie in the upper half-plane, and cannot be close to the unit circle.
- $m_{10} > 0$ and $m_{12} > 0$, or $m_{12} > 0$ and $m_2 > 0$: all possible values of $\boldsymbol{k_m}$ lie in the right half-plane, and cannot be close to the unit circle.

The only remaining possibilities are either $m_6 > 0$ and $m_8 > 0$, or $m_8 > 0$ and $m_{10} > 0$. However, for every combination of m_j in one configuration (m_1, m_3, m_6, m_8), there is an equivalent combination in the other configuration (m_1, m_3, m_8, m_{10}) that has equal distance to the unit circle: $m'_1 = m_3$, $m'_3 = m_1$, $m'_6 = m_{10}$, $m'_8 = m_8$, $m'_{10} = m_6$. So we need only consider cases where (m_1, m_3, m_8, m_{10}) are nonzero.

Looping over all possible combinations of (m_1, m_3, m_8, m_{10}) with $m_1 + m_3 + m_8 + m_{10} \leq N$ gives an order N^4 algorithm, but this can be improved as follows.

The vectors $\boldsymbol{k}_1 = (1, 0)$ and $\boldsymbol{k}_{10} = (0, -1)$. If $\boldsymbol{k_m}$ is to be close to the unit circle, $m_3\boldsymbol{k}_3 + m_8\boldsymbol{k}_8$ must lie in or near the upper left quadrant of the wavevector plane (positive k_y, negative k_x), or at least within the range $k_x < 2$ and $k_y > -2$. Furthermore, for given m_3 and m_8, the values of m_1 and m_{10} for which $\boldsymbol{k_m}$ can lie close to the unit circle are quite restricted: $m_1\boldsymbol{k}_1 + m_{10}\boldsymbol{k}_{10} = (m_1, -m_{10})$ must be near the vector $-m_3\boldsymbol{k}_3 - m_8\boldsymbol{k}_8$.

So instead of looping over all possible combinations of (m_1, m_3, m_8, m_{10}), it is only necessary to loop over (m_3, m_8) and check values of m_1 close to (within 2 of) the negative of the x component of $m_3\boldsymbol{k}_3 + m_8\boldsymbol{k}_8$, and values of m_{10} close to (within 2 of) the y component of $m_3\boldsymbol{k}_3 + m_8\boldsymbol{k}_8$, which results in an order N^2 algorithm.

The algorithm can be tidied up a little, and similar arguments can be applied in the cases $Q = 8$ and (with a little more difficulty) $Q = 10$. When $Q \geq 14$, only order N^4 or slower algorithms are possible, based on the same ideas. These methods were used to generate the data in figure 4.